Rotation of Nonspherical Particles in Turbulent Channel Flow

Lihao Zhao,[1] Niranjan Reddy Challabotla,[1] Helge I. Andersson,[1] and Evan A. Variano[2]
[1]Department of Energy and Process Engineering, Norwegian University of Science and Technology, 7491 Trondheim, Norway
[2]Department of Civil and Environmental Engineering, University of California, Berkeley, California 94720, USA
(Received 25 February 2015; published 11 December 2015)

The effects of particle inertia, particle shape, and fluid shear on particle rotation are examined using direct numerical simulation of turbulent channel flow. Particles at the channel center (nearly isotropic turbulence) and near the wall (highly sheared flow) show different rotation patterns and surprisingly different effects of particle inertia. Oblate particles at the center tend to rotate orthogonally to their symmetry axes, whereas prolate particles rotate around their symmetry axes. This trend is weakened by increasing inertia so that highly inertial oblate spheroids rotate nearly isotropically about their principle axes at the channel center. Near the walls, inertia does not move the rotation of spheroids towards isotropy but, rather, reverses the trend, causing oblate spheroids to rotate strongly about their symmetry axes and prolate spheroids to rotate normal to their symmetry axes. The observed phenomena are mostly ascribed to preferential orientations of the spheroids.

DOI: 10.1103/PhysRevLett.115.244501 PACS numbers: 47.55.Kf, 47.27.ek, 47.27.nd

Aspherical particles are encountered in many natural and industrial processes: sediment transport in estuaries [1], ice crystals in the atmosphere [2,3], pulp fibers in paper making [4], and planktonic and swimming microorganisms in the ocean [5,6]. Furthermore, all of these example particles have non-negligible inertia, meaning that they do not instantly adjust to equilibrium with the dynamic behavior of the fluids in which they are embedded.

Previous studies have revealed the dynamics of inertia-free aspherical particles in homogeneous isotropic turbulence [7–14]. These have shown particles to preferentially align with respect to fluid vorticity and/or strain, which causes particle rotation to differ from that of fluid parcels, even though the particles are noninertial. Specifically, rods tend to align their symmetry axis with the local fluid vorticity vector, which leads them to rotate preferentially around their symmetry axis [9]. Disks align one of their long axes with the local fluid vorticity, leading to minimal rotation about their symmetry axis. In other words, "rods spin and disks tumble" [13].

Inertial particles have been investigated in homogeneous isotropic turbulence [15,16] and (more commonly) in turbulent channel flow [17–22]. Analysis has focused on particle clustering, turbophoresis, and particle motion. The analyses of particle motion in channel flow have been conducted entirely in the laboratory frame and have not yet considered the interesting behavior that can be seen by examining particle motion with respect to their principle axes.

These recent studies leave the following questions unanswered: To what extent will particle inertia affect the partition between tumbling and spinning in homogeneous isotropic turbulence? How does strong fluid shear change the tumbling and spinning? Does the tumbling and spinning of spheroids seen in isotropic turbulence also occur in the nearly isotropic core region of a turbulent channel flow? Finally, do aspherical particles orient preferentially, and if so, where?

In this Letter, we, therefore, examine the motion of aspherical inertial particles in turbulent channel flow with respect to their local axes. Channel flow allows us to examine the transition in behavior from nearly isotropic turbulence at the channel center to highly sheared anisotropic turbulence near the channel wall. In this flow, we consider the combined effects of particle shape (from oblate to prolate) and particle inertia. These results serve to extend and unite the hitherto disparate studies of channel flow and homogeneous isotropic turbulence.

Direct numerical simulation (DNS) with a pseudospectral method was performed to simulate a turbulent channel flow closely matching that of Kim *et al.* [23]. The flow is periodic in streamwise (x) and cross-stream (y) directions and has no-slip boundaries at the top and bottom walls. The Reynolds number is based on the wall friction velocity (u_τ), and the channel half-height (h) is 180 [18,21]. We consider two regions of the flow: a region near the channel center ($z^+ = 180$), where turbulence is nearly homogeneous and isotropic [24], and a region near the channel wall ($z^+ = 10$), which is in the buffer layer. At this location, the flow has a strong mean shear, large values for the Reynolds shear stress $-\langle uw \rangle$, and the velocity fluctuation magnitudes are maximized.

In the simulation, swarms of 500 000 noninteracting particles of each type are randomly injected into the fully developed turbulent channel flow at $t^+ = 0$ (t^+ is normalized by the wall-shear time scale νu_τ^{-2}), and the statistics are computed by averaging instantaneous data in homogeneous directions over a time window of $7200 < t^+ < 9000$ for inertial spheroids and $720 < t^+ < 2520$ for tracer

spheroids. The particle motion is computed using a one-way coupling scheme, in which Lagrangian particle paths in the Eulerian DNS field are determined using Newtonian mechanics. Forces and torques acting on a spheroid are taken from Brenner [25] and Jeffery [26], respectively, who give expressions assuming steady flow in the creeping flow regime. These drag-type forces are the only ones considered in the present study; gravity, added mass force, and history force are considered second order in importance. All particle dimensions are smaller than (or on the order of) the Kolmogorov length scale. The numerical methods and validation are described in Ref. [18] for prolate spheroids and Ref. [21] for oblate spheroids.

The translational Stokes numbers (St) are derived based on a particle time scale (τ) that assumes isotropic particle orientation relative to the ambient flow [18,21,27]:

$$\tau = \begin{cases} \frac{2Da^2}{9\nu}\frac{\lambda\{\pi - 2tan^{-1}[\lambda(1-\lambda^2)^{-1/2}]\}}{2(1-\lambda^2)^{\frac{1}{2}}} & \lambda \le 1 \\ \frac{2Da^2}{9\nu}\frac{\lambda \ln\left[\lambda+\sqrt{(\lambda^2-1)}\right]}{\sqrt{(\lambda^2-1)}} & \lambda \ge 1 \end{cases}, \quad (1)$$

where D is the density ratio between particle and fluid, and the aspect ratio $\lambda = 2c/2a$ is the ratio between the symmetry axis (length $2c$) and the two equal axes (length $2a$). Particles are selected to sample a range of λ values, from 0.01 (oblate) to 50 (prolate). For each λ value, three different particle densities are considered in order to sample a range of translational Stokes numbers. The Stokes numbers are set to zero, 0.074, and 2.222 (based on the Kolmogorov time scale τ_η at the channel centerline) or, equivalently, to zero, 1, and 30 (based on the channel wall-shear time scale).

The rotational Stokes numbers differ from the translational ones, because the time scale over which a particle reaches rotational equilibrium with the surrounding flow depends on the moment-of-inertia tensor. A first-order calculation of rotational response time can be made by considering a flow with zero fluid strain and using the steady-flow torque equations of Jeffery [26] to examine a particle approaching equilibrium with the local flow. From this, we see that spheroids approach rotational equilibrium faster than they approach translational equilibrium, regardless of particle shape and which principle axis is being considered. For example, given three spheroids with identical translational relaxation times τ that are coming to rotational equilibrium about their symmetry axis (z'), a prolate spheroid (aspect ratio $\lambda = 10$) will come to rotational equilibrium in 0.13τ, a sphere (aspect ratio $\lambda = 1$) in 0.3τ, and an oblate spheroid (aspect ratio $\lambda = 0.1$) in 0.4τ.

Let ω_i and Ω_i denote the angular velocity of a particle and a fluid element, respectively. We decompose the particle enstrophy ($\langle\omega_i\omega_i\rangle$) into "spin" and "tumbling" components, where spin describes only the rotation about a spheroid's symmetry axis (z') as $\langle\omega_{z'}\omega_{z'}\rangle$, and tumbling describes rotation about the other two axes (x' and y') as $\langle\omega_{x'}\omega_{x'}\rangle + \langle\omega_{y'}\omega_{y'}\rangle$. We observe from Fig. 1(a) that for $St = 0$ particles at the channel center, oblate spheroids tumble more than prolate spheroids; this result is consistent with the previous findings in homogeneous isotropic turbulence [9–11,13]. The other results in Fig. 1 show that inertia reduces particle enstrophy and makes rotation more isotropic with respect to the particles' principle axes, i.e., weakening the tendency of disks to preferentially tumble and rods to preferentially spin. Figure 1(c) also shows that local fluid enstrophy decreases with increasing particle inertia, indicating that inertial spheroids preferentially sample regions of low fluid vorticity, in contrast to tracers which are distributed randomly.

Spheroids' tendency to emphasize specific components of rotation can be explained by examining their orientation relative to fluid vorticity; the inner product between a particle's orientation vector and the local fluid vorticity vector yields an angle α shown in Fig. 2 for the nearly isotropic channel center. For $St = 0$ particles, the results replicate previous observations [8–14] for disks and rods. Disks tend to align with their symmetry axis (z') orthogonal to the fluid vorticity, causing strong tumbling [8–14] and

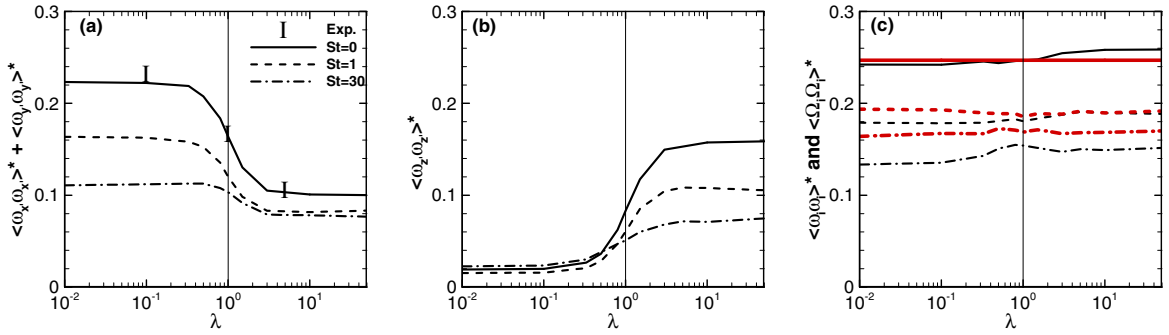

FIG. 1 (color online). Channel-center results of (a) tumbling components, (b) spinning component, and (c) total particle enstrophy versus aspect ratio λ. Tumbling (a) has a strong response to inertia for disks and a weak response to inertia for rods. Spinning (b) has a weak response to inertia for disks and a strong response to inertia for rods. The black lines and thick red lines (c) represent the particle enstrophy $\langle\omega_i\omega_i\rangle$ and the fluid enstrophy $\langle\Omega_i\Omega_i\rangle$ sampled by the particles (Eulerian fluid enstrophy is $0.247\tau_\eta^{-2}$), respectively. Star quantities are normalized with Kolmogorov time scale τ_η; symbols in (a) are laboratory data by Parsa *et al.* [9] and Marcus *et al.* [10].

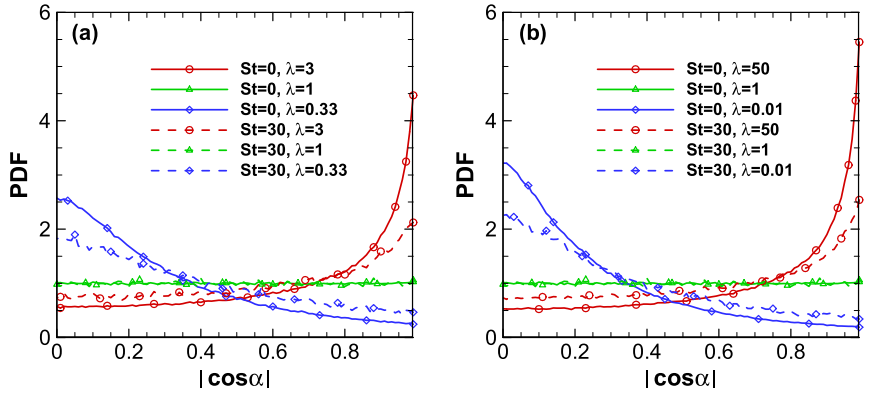

FIG. 2 (color online). Channel-center distributions of particles' instantaneous alignment α with local fluid vorticity for (a) moderate asphericity and (b) extreme asphericity. Solid lines are inertia-free; dashed lines are inertial. Blue lines with diamond symbols are disks, red lines with circle symbols are rods, and green lines with triangle symbols are spheres.

weak spinning [11,13]. Rods align parallel to local vorticity [8,10–14] and, thus, spin along with it. The most recent studies [12–14] also showed that the preferential alignment of the major axis of tracer spheroids in the direction of the fluid vorticity vector arises because both independently tend to align with the strongest Lagrangian stretching direction. This alignment effect becomes slightly stronger for particles with greater departure from sphericity, which can be seen by comparing corresponding lines between Figs. 2(a)and 2(b).

Increased particle inertia weakens the alignment effect for all shapes studied, making rods less likely to emphasize spinning and disks less likely to emphasize tumbling (Fig. 1). This tendency could be caused by two mechanisms. First, when inertial spheroids avoid sampling regions of strong vorticity [see Fig. 1(c)], they also avoid regions where they will experience strong alignment, because strain-vorticity alignment is strongest in the presence of strong vorticity [12,13]. Second, because inertial particles do not follow the flow passively [20,28,29] (even an inertial sphere does not rotate along with the local fluid rotation [28]), it is likely that spheroids' inertia induces a temporal filter on the rotational motion and, thus, prevents the particle from extracting all available vorticity from the flow. Roughly, inertial spheroids will not align with or rotate along with motions whose duration is less than the particle relaxation time, which leads to less alignment and less emphasis on either tumbling or spinning.

Results for the near-wall region ($z^+ = 10$) are seen in Fig. 3, which is analogous to Fig. 1 but shows very different behavior. Weakly inertial (St $= 0$ and 1) disks tumble, especially when their aspect ratio is near 1, but they also exhibit a fair amount of spinning as well. Strongly inertial disks almost exclusively spin. Short and weakly inertial rods almost equally spin and tumble, and the amount of spinning increases with length. As inertia increases, both short and long rods emphasize tumbling more than spinning, which indicates that the inertia effect is more dominant than the shape effect.

Similar to the case of the channel center, particle enstrophy near the wall [black lines in Fig. 3(c)] is less than that of the surrounding fluid [thick red lines in Fig. 3(c)]. Unlike the channel center, however, near-wall particle enstrophy is strongly dependent on shape. Stronger asphericity leads to lower particle enstrophy. The effect of inertia

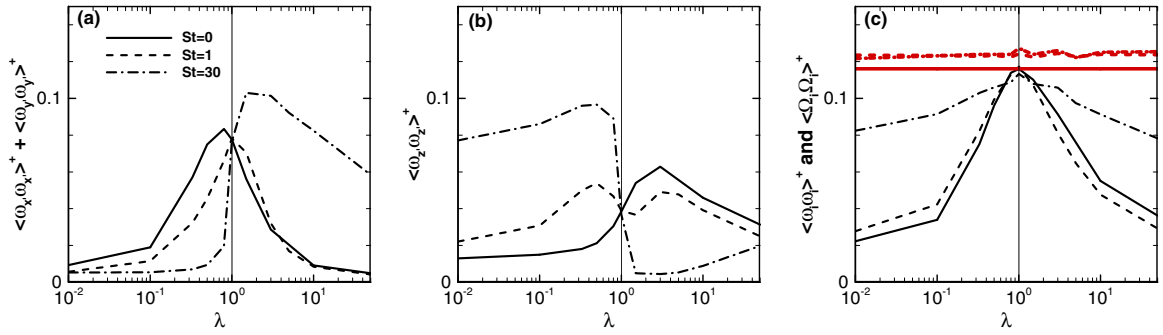

FIG. 3 (color online). Near-wall results of the (a) tumbling and (b) spinning component of particle enstrophy and (c) total particle and fluid enstrophy. The black lines and thick red lines (c) represent the particle enstrophy $\langle \omega_i \omega_i \rangle$ and the fluid enstrophy $\langle \Omega_i \Omega_i \rangle$ sampled by the particles, respectively. Plus quantities are normalized by $\nu^{-2} u_\tau^4$.

in the near-wall region (enstrophy increasing with particle inertia) is opposite to the case seen at the channel center (enstrophy decreasing with particle inertia). The thick red lines in Fig. 3(c) provide a partial explanation of this effect, showing that particle inertia causes spheroids to preferentially sample high-vorticity flow structures in the near-wall region. Such preferential sampling is related to particle clustering, and near-wall clustering has been discussed previously in the literature [20].

The preferential sampling seen near the wall is opposite to that at the channel center, suggesting that different mechanisms dominate particle clustering in isotropic turbulence than in highly sheared near-wall turbulence. Because both types of preferential sampling are shape independent [the thick red lines are nearly flat in Figs. 1(c) and 3(c)], our data suggest that the strong shape dependence of particle enstrophy in the near-wall region is caused by more than particle clustering. To explain this behavior, we examine spheroid alignment relative to local vorticity (Fig. 4). When their inertia is increased, disks will switch from perpendicular (St = 0) to parallel (St = 30) alignment relative to fluid vorticity [21] and, therefore, emphasize spinning induced by the mean fluid shear [Fig. 3(b)]. A similar effect is seen for rods: when their inertia is increased, rods switch from parallel (or partly parallel) [19,20,30] to perpendicular alignment relative to vorticity, thereby emphasizing tumbling [Fig. 3(a)].

Alignment between spheroids and fluid vorticity is caused by a different mechanism near the wall than in the channel center. Near the channel wall, the large mean velocity gradient $d\langle U\rangle/dz$ provides a strong mean vorticity in the cross-stream y direction, and the local turbulence field is anisotropic, with vorticity fluctuations being strongest in the y direction and weakest in the x direction [23,24]. Recent work on the rotational dynamics of a single oblate spheroid in a uniform shear flow revises the concept of Jeffery orbits to show that an inertial disk eventually rotates in the shear plane irrespective of its initial conditions [31]. Similarly, a prolate spheroid drifts towards rotation in the x-z plane [32]. Similar behaviors of inertial spheroids (St = 30) in wall turbulence are observed here; i.e., disks emphasize spinning in the x-z plane (aligned with the vorticity vector), whereas rods emphasize tumbling in the x-z plane (aligned normal to the vorticity vector). These observations suggest that inertial spheroids in near-wall turbulence behave just like those in a linear shear flow. The likely reason is that the inertial spheroids filter the effect of small-scale turbulent fluctuations and only respond effectively to the largest flow structures and the mean shear. In other words, inertia causes the mean-shear effect to dominate the rotational dynamics of inertial spheroids in wall turbulence.

Tracer spheroids in the wall region, in contrast to inertial spheroids discussed above, exhibit more complex rotational dynamics, and their preferential alignment is caused by other mechanisms. First, we observe from Fig. 4(b) that inertia-free spheroids tend to align with their symmetry axis normal to the vorticity vector, typically in the streamwise direction. This preferential alignment is consistent with numerical [18–22] and experimental findings [30] in wall turbulence. However, the preferential orientation of the St = 0 spheroids in the near-wall region cannot explain the emphasized tumbling or spinning; e.g., both tracer disks and rods only weakly tumble [Fig. 3(a)] even though they both align [Fig. 4(b)] normal to mean vorticity vector. This observation suggests that an inertia-free spheroid does not respond efficiently to mean shear. Recently, Voth [33] argued that a weakly inertial oblate spheroid aligned near the wall-normal direction will spend a long time in this orientation before tumbling. Challabotla *et al.* [34] similarly observed that prolate tracers with their symmetry axis almost aligned in the streamwise direction rarely tumble, and the observed orientation and rotation of tracer spheroids in the viscous sublayer was qualitatively consistent with spheroids in Jeffery orbits in linear shear flow. Thus, we conclude that the weak tumbling and spinning for inertia-free spheroids with a high aspect ratio can be attributed to Jeffery-like orbiting. However, the mechanism

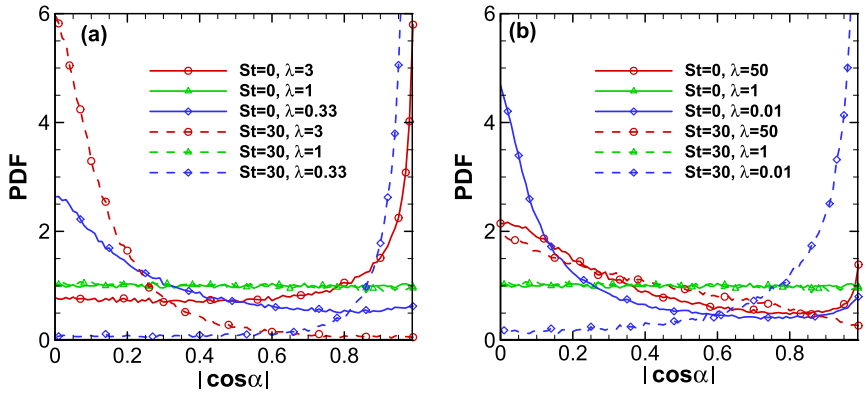

FIG. 4 (color online). Near-wall distributions of particles' instantaneous alignment α with local fluid vorticity for (a) moderate asphericity and (b) extreme asphericity. Solid lines are inertia-free; dashed lines are inertial. Blue lines with diamond symbols are disks, red lines with circle symbols are rods, and green lines with triangle symbols are spheres.

that aligns such particles preferentially in that orientation remains an open question.

A possible explanation for the preferential alignment is suggested by recent findings concerning preferential alignment of a spheroid's major axis in the Lagrangian strongest stretching direction in homogeneous isotropic turbulence [12,13]. Lagrangian coherent structures (LCSs) [35] act as organizers of transport in fluid flows having a clear impact on the particle trajectories [36]. Near-wall LCSs have been studied in channel flow turbulence [36–38] and "curved legs" of the coherent streamwise structure inclined in the streamwise direction with about 20° were reported [38]. In the present study, the major axis of the inertia-free spheroids and the near-wall quasistreamwise vortices' vector are both almost aligned in the streamwise x direction. Just as in the channel center, this preferred alignment of the spheroids with the quasistreamwise vortices makes disks tumble more than spin and rods spin more than tumble. We, therefore, hypothesize that the light spheroids are captured by, and partially move along with, the coherent vortices in the wall turbulence and, therefore, preferentially align in the streamwise direction.

In conclusion, we have explored rotation about the principle axes of spheroids suspended in turbulent channel flow. In the channel center, we have found that inertia-free spheroids were tumbling and spinning just as in homogeneous isotropic turbulence [9,10], whereas inertia reduced the preferential spinning or tumbling and led to a more isotropic rotation. This observation is likely caused by preferential clustering of the inertial spheroids in low-vorticity regions and inertial filtering of the local vorticity.

Spheroids in the wall region are affected both by mean shear and anisotropic fluid vorticity, and their rotational behavior is totally different from at channel center. We argue that inertial spheroids respond strongly to the mean shear, whereas inertia-free spheroids do not. The complex rotation of these tracers is a consequence of the preferential orientation of the inertia-free spheroids. We hypothesize that the preferential orientation of these particles is caused by interactions with the coherent vortex structures in wall turbulence.

This material is based upon work supported by the National Science Foundation under Grant No. OCE-1334788 (E. V.) and by the Research Council of Norway under Project No. 213917/F20 (H. I. A.) and Programme for Supercomputing. Support and motivation was provided by the Peder Sather Center for Advanced Study at University of California, Berkeley.

[1] A. J. Mehta, *An Introduction to Hydraulics of Fine Sediment Transport* (World Scientific Publishing Company, Singapore, 2013).
[2] R. A. Shaw, Annu. Rev. Fluid Mech. **35**, 183 (2003).
[3] A. Korolev and G. Isaac, J. Atmos. Sci. **60**, 1795 (2003).
[4] F. Lundell, L. D. Söderberg, and P. H. Alfredsson, Annu. Rev. Fluid Mech. **43**, 195 (2011).
[5] J. S. Guasto, R. Rusconi, and R. Stocker, Annu. Rev. Fluid Mech. **44**, 373 (2012).
[6] T. J. Pedley and J. O. Kessler, Annu. Rev. Fluid Mech. **24**, 313 (1992).
[7] M. Shin and D. L. Koch, J. Fluid Mech. **540**, 143 (2005).
[8] A. Pumir and M. Wilkinson, New J. Phys. **13**, 093030 (2011).
[9] S. Parsa, E. Calzavarini, F. Toschi, and G. A. Voth, Phys. Rev. Lett. **109**, 134501 (2012).
[10] G. G. Marcus, S. Parsa, S. Kramel, R. Ni, and G. A. Voth, New J. Phys. **16**, 102001 (2014).
[11] K. Gustavsson, J. Einarsson, and B. Mehlig, Phys. Rev. Lett. **112**, 014501 (2014).
[12] R. Ni, N. T. Ouellette, and G. A. Voth, J. Fluid Mech. **743**, R3 (2014).
[13] M. Byron, J. Einarsson, K. Gustavsson, G. Voth, B. Mehlig, and E. A. Variano, Phys. Fluids **27**, 035101 (2015).
[14] R. Ni, S. Kramel, N. T. Ouellette, and G. A. Voth, J. Fluid Mech. **766**, 202 (2015).
[15] C. Siewert, R. P. J. Kunnen, M. Meinke, and W. Schröder, Atmos. Res. **142**, 45 (2014).
[16] G. Bellani, M. L. Byron, A. G. Collignon, C. R. Meyer, and E. A. Variano, J. Fluid Mech. **712**, 41 (2012).
[17] H. Zhang, G. Ahmadi, F.-G. Fan, and J. B. McLaughlin, Int. J. Multiphase Flow **27**, 971 (2001).
[18] P. H. Mortensen, H. I. Andersson, J. J. J. Gillissen, and B. J. Boersma, Phys. Fluids **20**, 093302 (2008).
[19] C. Marchioli, M. Fantoni, and A. Soldati, Phys. Fluids **22**, 033301 (2010).
[20] L. Zhao, C. Marchioli, and H. I. Andersson, Phys. Fluids **26**, 063302 (2014).
[21] N. R. Challabotla, L. Zhao, and H. I. Andersson, J. Fluid Mech. **766**, R2 (2015).
[22] C. Marchioli and A. Soldati, Acta Mech. **224**, 2311 (2013).
[23] J. Kim, P. Moin, and R. Moser, J. Fluid Mech. **177**, 133 (1987).
[24] H. I. Andersson, L. Zhao, and E. Variano, ASME J. Fluids Eng. **137**, 084503 (2015).
[25] H. Brenner, Chem. Eng. Sci. **19**, 703 (1964).
[26] G. B. Jeffery, Proc. R. Soc. A **102**, 161 (1922).
[27] M. Shapiro and M. Goldenberg, J. Aerosol Sci. **24**, 65 (1993).
[28] P. H. Mortensen, H. I. Andersson, J. J. J. Gillissen, and B. J. Boersma, Phys. Fluids **19**, 078109 (2007).
[29] L. Zhao, C. Marchioli, and H. I. Andersson, Phys. Fluids **24**, 021705 (2012).
[30] A. Abbasi Hoseini, F. Lundell, and H. I. Andersson, Int. J. Multiphase Flow **76**, 13 (2015).
[31] N. R. Challabotla, C. Nilsen, and H. I. Andersson, Phys. Lett. A **379**, 157 (2015).
[32] F. Lundell and A. Carlsson, Phys. Rev. E **81**, 016323 (2010).
[33] G. Voth, J. Fluid Mech. **772**, 1 (2015).
[34] N. R. Challabotla, L. Zhao, and H. I. Andersson, Phys. Fluids **27**, 061703 (2015).
[35] G. Haller, Annu. Rev. Fluid Mech. **47**, 137 (2015).
[36] J. H. Bettencourt, C. Lopez, and E. Hernandez-Garcia. J. Phys. A **46**, 254022 (2013).
[37] M. A. Green, C. W. Rowley, and G. Haller, J. Fluid Mech. **572**, 111 (2007).
[38] Y. Yang and D. I. Pullin, J. Fluid Mech. **674**, 67 (2011).